ELSEVIER

Separation and Purification Technology 29 (2002) 217–227

Separation and Purification Technology

www.elsevier.com/locate/seppur

# The deduction of fine structural details of reverse osmosis hollow fiber membranes using surface force–pore flow model

Ani Idris [a], A.F. Ismail [a,*], S.J. Shilton [b], R. Roslina [a], M. Musa [c]

[a] *Membrane Research Unit, Faculty of Chemical and Natural Resources Engineering, Universiti Teknologi Malaysia, 81310 UTM, Skudai, Johor, Malaysia*

[b] *Department of Chemical and Process Engineering, University of Strathclyde, James Weir Building, 75 Montrose Street, Glasgow G1 1XJ, Scotland, UK*

[c] *Department of Applied Mechanics, Faculty of Mechanical Engineering, Universiti Teknologi Malaysia, 81310 UTM, Skudai, Johor, Malaysia*

Received 23 January 2002; received in revised form 29 March 2002; accepted 6 May 2002

**Abstract**

In order to elucidate the relationship between the dope extrusion shear rate and membrane performance, sodium chloride transfer through the asymmetric cellulose acetate reverse osmosis hollow fiber membranes is modeled, allowing fine details of the fiber structure to be deduced from the NaCl–$H_2O$ rejection characteristics. The structural information such as the pore size radius and skin thickness of the active layer deduced from the sodium chloride separation experimental data and surface force–pore flow model (SF–PF) is then used to interpret the relationship between the rheological conditions during spinning and membrane performance. The modeling results revealed that increased extrusion shear rate would decrease both pore size and thickness of the active layer, thus increasing the separation performance of the RO hollow fiber membranes. 

*Keywords:* Spinning rheology; Reverse osmosis; Hollow fiber; Molecular orientation; Skin and structure

## Nomenclature

| | |
|---|---|
| $c_A$ | molar concentration of solute (gmol/m$^3$) |
| $c$ | molar concentration of solution (mol/m$^3$) |
| $C_A$ | dimensionless solute concentration at the pore outlet |
| $D_{AB}$ | diffusivity of solute in the water (m$^2$/s) |

* Corresponding author. Tel.: +60-7-550-5392; fax: +60-7-558-1463
*E-mail address:* afauzi@.utm.my (A.F. Ismail).

1383-5866/02/$ - see front matter 
PII: S1383-5866(02)00081-3

| | |
|---|---|
| $D_w$ | water molecule radius (m) |
| $f'$ | true value of solute separation by membrane pore |
| $f$ | solute separation based on the solute concentration in the bulk feed |
| $g$ | solution density (kg/m$^3$) |
| $k$ | mass transfer coefficient on the high pressure side of the membrane (m/s) |
| $M_B$ | molecular weight (kg/mol) |
| $\Delta p$ | pressure difference across membrane (Pa) |
| $p$ | pressure (Pa) |
| $q_w$ | permeation rate of pure water through a single pore (kg/s) |
| $Q_w$ | permeation rate of pure water through pores (kg/s) |
| $r$ | radial distance (m) |
| $R$ | gas constant, 8.314 J/mol K |
| $R_b$ | membrane pore radius (m) |
| $R_a$ | water channel radius (m) |
| $S$ | surface area of membranes (m$^2$) |
| $T$ | absolute temperature (K) |
| $v_B$ | molar volume of water (m$^3$/mol) |
| $v$ | permeation velocity of product solution (m/s) |
| $X_A$ | mole fraction of the solute |

*Greek letters*

| | |
|---|---|
| $\varepsilon_p$ | porosity of membrane |
| $\delta$ | the membrane thickness or effective pore length (m) |
| $\rho$ | dimensionless quantity defined by the first equation below |
| $\alpha(\rho)$ | dimensionless solution velocity profile in the pore |
| $\chi_{AB}$ | solute–solvent friction function |
| $\eta$ | viscosity of the solution in the pore (Pa s $= 0.8941 \times 10^{-3}$) |
| $\beta_1$ | dimensionless solution viscosity |
| $\beta_2$ | dimensionless operating pressure |
| $\alpha$ | activity coefficient |
| $\Phi(\rho)$ | dimensionless potential function |
| $\phi$ | potential in the interfacial force field |
| $b(\rho)$ | dimensionless friction function |
| $\chi_{AM}$ | quantity characterizing the friction between solute and membrane pore wall (J s/m$^2$ mol) |
| $\chi_{AB}$ | quantity characterizing the solute-solvent friction (J s/m$^2$ mol) |

*Subscripts*

| | |
|---|---|
| 1 | bulk feed solution on the high pressure side of membrane |
| 2 | concentrated boundary solution on high pressure side of membrane |
| 3 | membrane permeated product solution on the low-pressure side of membrane |

*Equations*

$\rho = r/R_a$

$C_A = c_{A3}/c_{A2}$

$\alpha(\rho) = u_B(r)\delta\chi_{AB}/RT$

$\chi_{AB} = RT/D_{AB}$
$\beta_1 = \eta/\chi_{AB}R_a^2 c_{A2}$
$\beta_2 = (p_2 - p_3)/RTc_{A2}$
$\Phi(\rho) = \phi(r)/RT$
$b(\rho) = [\chi_{AB} + \chi_{AM}]/\chi_{AB}$

## 1. Introduction

In addition to process design and simulation of the system, the properties and structure of the membrane itself is of primary importance if the membrane system is to be commercially viable. The effectiveness of the membrane system depends on the actual membrane structure, which in turn depends on the conditions during membrane fabrication. Knowledge of the fine structural details of the membrane at the microscopic level is a crucial factor in the development of the membrane itself and in the optimization of membrane fabrication techniques.

During these past years, investigations on the influence of shear rate on the morphology of hollow fiber gas separation membranes have been published [1–6]. The rate of shear experienced in the spinneret was found to have an effect on gas permeation performance of the hollow fiber membranes. However, all of the previous works were focused on gas hollow fiber membranes. Recently, some work has also been carried out to study the influence of shear rate on reverse osmosis hollow fiber membranes performance [7,8]. However, most of the previous works explained their experimental results qualitatively and literarily [2–8] with the exception of [1]. Shilton et. al [1] did mathematical modeling using the resistance approach which allows fine details of fiber structure such as the thickness of the active layer, surface porosity and solid polymer selectivity to be deduced from gas permeation data. The structural information is then used to interpret the relationship between spinning conditions and fiber properties. Recently Wang and Chung [9] determined the pore size of their gas membranes based on the resistance model and Poiseuille and Knudsen gas transport mechanisms to deduce the fine structural details and relates them to the fabrication conditions.

In ultrafiltration, Tam et al. [10] used the surface force–pore flow (SF–PF) model to describe solute transport through their laboratory prepared and commercially available polyethersulfone membranes. However, their work only involved the use of SF–PF model to provide estimation of the average pore radius and membrane porosity based on their experimental data.

In reverse osmosis membranes, various models have been proposed to describe the mass transport across the membrane, the earliest model developed by Kimura–Sourirajan based on the preferential sorption-capillary flow mechanism [11] and known widely as the Kimura–Sourirajan analysis (KSA). Since then, many researchers [12–17] had used the SF–PF model, which is a qualitative expression of the preferential sorption–capillary flow model to describe and predict the performance of reverse osmosis membranes. Most of their study involved the use of this model for the design and analysis of RO systems for single solute as well as multi-component systems [18–21] as well as to predict the permeator performance [22,23]. Voros et al. [24] and Velikova et al. [25] used the KSA to calculate transport parameters (i.e. mass transfer coefficients) as well as the permeability coefficients of water and salt in reverse osmosis membranes. These are useful for prediction of membrane performance and membrane characterization. Wang et al. [26] also used the KSA method to characterize the morphology and performance of cellulose acetate (formamide type) flat sheet membranes. Recently, Ani et al. [27] also used the KSA method to characterize the morphology of their flat sheet reverse osmosis membranes.

Based on these findings and to the best of our knowledge, no such mathematical analysis has been carried out for hollow fiber reverse osmosis membranes to quantitatively describe the influence of shear rate on the pore size and skin

thickness of hollow fiber membranes. In the current paper, we have used both the KSA analysis [11] and the basic SF–PF model [12,13] to estimate the pore size and skin thickness of our asymmetric cellulose acetate hollow fiber membranes. The structural information such as the pore size radius and skin thickness of the active layer is used to interpret the relationship between the extrusion shear rates and the membrane separation performance.

## 2. Theory

The determination of the pore size and the skin layer thickness is based on the preferential sorption-capillary flow mechanism, which involves the use of the Kimura–Sourirajan model and the SF–PF model. All parameters used in the foregoing equations are defined in the Nomenclature.

### 2.1. Mass transfer coefficient

Mass transfer for systems such as water–sodium chloride across the cellulose acetate reverse osmosis membranes is described by the preferentially sorption–capillary flow mechanism. The Kimura–Sourirajan model which is based on this mechanism, assumes that the solvent and solute fluxes through the membrane are mainly characterized by two phenomena: solute transport in terms of pure water permeability constant, and solute transport in terms of the solute transport parameter [12,13,24,25]. In this work, the mass transfer coefficient $k$ is calculated using the following equation

$$k = v \Big/ \ln\left[\frac{c_{A2} - c_{A3}}{c_{A1} - c_{A3}}\right] \tag{1}$$

The concentrations in the bulk of the feed, $c_{A1}$ and in the region at the membrane/solution boundary, $c_{A2}$ are different because of the concentration polarization phenomena. The product output concentration is designated as $c_{A3}$. Two different solute separations are defined; i.e.

$$f' = (c_{A2} - c_{A3})/c_{A2} \tag{2}$$

and

$$f = (c_{A1} - c_{A3})/c_{A1} \tag{3}$$

$f'$ is the true solute separation by the pore, $f$ is the apparent solute separation defined on the basis of the feed solute separations.

### 2.2. Surface force–pore flow model

Several assumptions were made when applying the SF–PF model:

1. the mechanism of separation is determined by interaction forces, friction forces and driving forces due to gradients in chemical potential of the solute and the solvent.
2. the pores of the membrane are assumed to be cylindrical and a solute potential field, which controls the radial distribution of solutes, exists within the pore.
3. a molecule thick layer of pure water is considered preferentially sorbed in the region immediately adjacent to membrane wall

A full description and derivation of all the mathematical equations is described elsewhere [12,13]. In brief, the SF–PF model used for the purpose in determining pore size are expressed in terms of solute separation and radial velocity profile for solvent flow in terms of dimensionless quantities defined by the equations in the Nomenclature. The solute separation $f'$, can be calculated by the equation

$$f' = 1 - \frac{\int_0^1 \{\exp[\alpha(\rho)]/1 + [b(\rho)/e^{-\Phi(\rho)}](\exp[\alpha(\rho)] - 1)\}\alpha(\rho)\rho\, d\rho}{\int_0^1 \alpha(\rho)\rho d\rho} \tag{4}$$

The radial velocity profile involved in the above equation can be calculated by solving the following differential equation

$$\frac{d^2\alpha(\rho)}{d\rho^2} + \frac{1}{\rho}\frac{d\alpha(\rho)}{d\rho} + \frac{\beta_2}{\beta_1} + \frac{1}{\beta_1}(1 - e^{-\Phi(\rho)})[C_A(\rho) - 1] - [b(\rho) - 1]\alpha(\rho)C_A(\rho)/\beta_1 = 0 \tag{5}$$

where

$$C_A(\rho) = \frac{\exp[\alpha(\rho)]}{1 + [b/e^{-\Phi(\rho)}](\exp[\alpha(\rho)] - 1)} \quad (6)$$

The boundary conditions for solving Eq. (5) are

$$\frac{d\alpha(\rho)}{d\rho} = 0 \quad \text{at } \rho = 0 \quad (7)$$

$$\alpha(\rho) = 0 \quad \text{at } \rho = 1 \quad (8)$$

For the case of pure water permeation through pore, the molar flow rate of the solvent water for one single pore, leads to the well-known Poiseuille equation

$$q_w = \frac{g}{M_B}\pi R_a^4(p_2 - p_3)/8\eta\delta \quad (9)$$

## 3. Experimentation

The experimental data used in this experiment has been reported in detail elsewhere [7]. In brief, a 27% cellulose acetate, 42.8% acetone and 29.2% formamide spinning dope was spun by forced convective dry/wet spinning technique described in Ref. [8]. In order to study the pure influence of shear rate, the dope extrusion rates are varied from 2.5 to 5.0 ml/min with a 0.5-ml increment. A total of 6 batches of hollow fibers are spun. The residence time is kept constant by adjusting the gap height. On extrusion from the spinneret (spinneret dimensions: OD 600 μm/ID 330 μm), the fiber passed through a cylindrical forced convection chamber (diameter 5 cm, heights 13, 16, 18, 21, 23 and 26 cm), which was flushed with 2 l/min of nitrogen gas. These fibers were then potted and tested using salt water of concentration 1000 ppm. The test for each batch of hollow fibers were repeated a minimum of 4 times to ensure reproducibility of results.

In order to know the shear rate experienced at the walls of the spinneret, rheological tests are carried out on the cellulose acetate spinning dope solution using the TA Instruments AR 1000 Rotational Rheometer. Rheological results indicate that the dope solution behaves as a shear thinning power law fluid: power law index 0.4823, power law constant 267.65 (Pa $s^n$). The flow profile in the spinneret for the different dope extrusion rates can be established by solving the flow equations for a power-law fluid in a concentric annulus [1,28]. This allows the shear rate experienced at the outer wall of the spinneret, i.e. the active layer region of the membrane, to be calculated. A summary of the shear rates generated at the outer spinneret walls are shown in Table 1.

### 3.1. Determination of the pore size on the membrane surface

The set of the experimental data in Table 2 show the influence of shear rate on hollow fiber membrane rejection rate, $f$ and flux. These data were obtained at an operating pressure of 689.29 kPa (6.8 atm) gauge, with $NaCl–H_2O$ feed solutions at solute concentration of 17.1 g mol/$m^3$ using hollow fiber cellulose acetate membranes spun at the different dope extrusion rates. In order to determine the pore size of the membrane, the mass transfer coefficient $k$ on the high pressure side of the membrane for the experimental conditions must be determined using the KSA analysis outlined in [13,24,25]. Based on the Kimura–Sourirajan Eq. (1), the mass transfer coefficient $k$ was calculated and found to be $1.2268 \times 10^{-8}$ m/s. This value was used throughout the rest of the calculation since the same experimental conditions were used. The pore sizes were calculated based on the steps outlined in [12,13] and the results were tabulated in Table 2.

### 3.2. Determination of the skin thickness

Once the pore size $R_b$ was obtained, the skin layer thickness was calculated based on the Poiseuille Eq. (9)

Table 1
Summary of shear rates generated at the outer spinneret walls

| DER (ml/min) | Shear rates ($s^{-1}$) |
|---|---|
| 2.5 | 11 233 |
| 3.0 | 13 479 |
| 3.5 | 15 726 |
| 4.0 | 17 972 |
| 4.5 | 20 219 |
| 5.0 | 22 465 |

Table 2
Modeling results; values of $R_b$, $A$ and $\delta$

| Shear rate ($s^{-1}$) | Flux $\times 10^4$ (kg/h) | $R_b \times 10^{10}$ (m) | $\delta$, Skin layer thickness (Å) | $f$ | $f'$ |
|---|---|---|---|---|---|
| 11 233 | 4.62 | 28 | 658.982 | 0.870 | 0.9680 |
| 11 233 | 3.30 | 28 | 922.574 | 0.865 | 0.9633 |
| 11 233 | 4.03 | 28 | 755.458 | 0.870 | 0.9676 |
| 11 233 | 4.33 | 28 | 703.117 | 0.862 | 0.9654 |
| 13 470 | 5.90 | 25 | 385.932 | 0.905 | 0.9758. |
| 13 470 | 4.90 | 25 | 392.586 | 0.890 | 0.9794 |
| 13 470 | 5.80 | 25 | 464.694 | 0.920 | 0.9809 |
| 13 470 | 5.00 | 25 | 455.400 | 0.851 | 0.9779 |
| 15 727 | 8.72 | 22.5 | 246.551 | 0.926 | 0.9903 |
| 15 727 | 5.65 | 22.5 | 348.213 | 0.941 | 0.9845 |
| 15 727 | 6.16 | 22.5 | 379.645 | 0.924 | 0.9868 |
| 15 727 | 6.66 | 22.5 | 322.071 | 0.926 | 0.9864 |
| 17 972 | 11.03 | 20 | 151.111 | 0.955 | 0.9956 |
| 17 972 | 8.86 | 20 | 175.671 | 0.954 | 0.9931 |
| 17 972 | 8.14 | 20 | 191.209 | 0.955 | 0.9919 |
| 17 972 | 7.81 | 20 | 199.288 | 0.942 | 0.9913 |
| 20 219 | 8.31 | 22 | 252.719 | 0.923 | 0.9890 |
| 20 219 | 1.13 | 22 | 321.364 | 0.912 | 0.9935 |
| 20 219 | 5.78 | 22 | 223.524 | 0.915 | 0.9855 |
| 20 219 | 7.35 | 22 | 164.379 | 0.908 | 0.9870 |
| 22 465 | 8.61 | 20 | 168.630 | 0.905 | 0.9892 |
| 22 465 | 9.31 | 20 | 155.951 | 0.927 | 0.9925 |
| 22 465 | 4.98 | 20 | 164.243 | 0.896 | 0.9792 |
| 22 465 | 8.84 | 20 | 197.807 | 0.865 | 0.9897 |

$$\delta = \frac{g}{M_B}\pi R_a^4 (p_2 - p_3)/8\eta q_w \quad (10)$$

No surface pores could be visually observed in the skins of any of the fibers under SEM at magnifications of up to 50 000. This indicates that the porosity of the membrane, $\varepsilon_p$ is generally less than $1 \times 10^{-6}$. The SFPF model assumes that the transported water and solute takes place through cylindrical pores of radius, $R_b$, equivalent to the summation of the water channel radius and the water molecules radius. In the SFPF model it is also assumed that there is an area into which the center of the water molecule cannot enter due to the collision with the membrane pore; thus two radius, $R_b$ and $R_a$ are defined as $R_a = R_b - D_w$ [10,11,29]. The skin thickness in Eq. (11) can then be rearranged and written as

$$\delta = \frac{\frac{g}{M_B}(R_b - D_w)^4 (p_2 - p_3)\varepsilon_p S}{8\eta (R_b)^2 Q_w} \quad (11)$$

The operating pressure is 689.29 kPa (6.8 atm) gauge whilst the water molecule radius, $D_w = 0.87 \times 10^{-10}$ m. By inserting all the numerical values into Eq. (11) will enable all the skin thickness of the various membranes spun under different extrusion shear rates to be calculated and these values are tabulated in Table 2.

## 4. Pore modeling results

Table 2 shows the pore modeling results; values of the pore size $R_b$ and skin layer thickness, $\delta$ against the performance of the membranes. These values represent the fine structural details of the membrane. The delicate nature of the membranes surface also results in susceptibility to random pinholes or imperfections. Thus subtle

alterations in process conditions, practical procedures or handling in spinning, washing, post treatment, drying, potting up or salt water testing inevitably cause variations in the rejection rate

performance of the hollow fibers. However, it was proven statistically by regression analysis and analysis of variance (ANOVA) that there is a strong correlation between the extrusion shear rate and the rejection rate of RO hollow fiber membranes [7]. Thus, the overall trend data reasonably represents the nature of the rheological effects on the rejection properties of the hollow fibers and these values are fed into the SF–PF model.

The change in the fine structural details can be clearly viewed by plotting the skin layer thickness of the membrane versus the extrusion shear rate as shown in Fig. 1. The graph shows that there is a decrease in skin thickness of the membrane as the extrusion shear rate increases. It is also observed from Table 2 that the pore size of the membranes decreases as the extrusion shear rate increases. No pores could be visually observed in the skins of any of the fibers by scanning electron microscopy even up to magnifications of 50 000. Thus, the porosity of $1 \times 10^{-6}$ assumed enabled the pore modeling to propose sensible structural details, which represented the rejection properties of the membranes. In addition, the calculated pore size obtained seems to be reasonably accurate, the largest pore size being 28 Å at low extrusion rate of 11 233 $s^{-1}$ and slowly decreases to 20 Å. Further increase of extrusion rate beyond 17 972 $s^{-1}$ no longer results in the reduction of pore size.

The effect of the fine structural details such as the skin thickness on the rejection rate of the membranes can also be seen in Fig. 1. It can be seen as the extrusion shear rates increases, rejection rate increases; the skin thickness decreases from the region of 800 to 200 Å. At the highest level of shear rate, the apparent active layer thickness is approximately in the region of 160 to 200 Å. At this point, to increase confidence in the veracity of the modeling, it is worth noting that the predicted values of the active thickness can be verified from the SEM micrographs. Fig. 2(a,b) show the existence of a distinct active layer at the outer skin of membranes spun at lower extrusion shear rates of 13 470 and 15 727 $s^{-1}$, respectively. This distinct layer thickness reduces with the increase in extrusion shear rates. The apparent active layer thickness calculated lies within this distinct layer and this layer reduces as the distinct layer reduces. At high extrusion shear rates of 17 972 and 22 465 $s^{-1}$ the active skin layer becomes very thin so much so that no such discrete layer can be identified as can be seen in Fig. 2(c,d). At this point the rejection rate reaches its maximum value. Beyond this point a further increase in shear rate will not cause the skin thickness to reduce further. This trend is shown very clearly in Fig. 1.

The influence of the skin thickness on the flux rate can be observed by plotting a graph of flux rate, skin thickness versus extrusion shear rates as shown in Fig. 3. As extrusion shear rate increases, the active skin thickness decreases and this causes an increase in the flux rate.

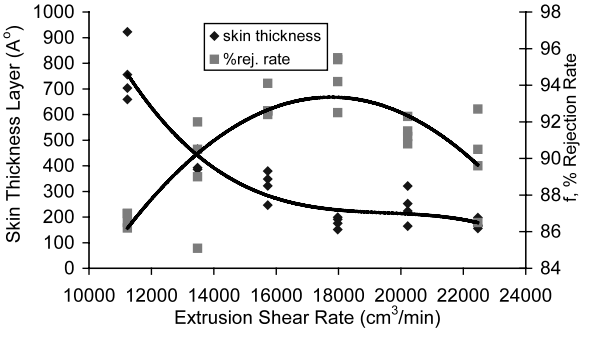


Fig. 1. Skin layer thickness and percentage rejection rate versus extrusion shear rate.

## 5. Discussion

The modeling results provided interesting structural details of the membrane. The SF–PF model allows the pore size of the membrane to be calculated and this pore size can then be substituted into the Poiseuille equation so as to have an estimate of the active skin layer thickness. Modeling results revealed that the hollow fiber membranes spun at low dope extrusion shear rates possess larger pore sizes and thicker skins. As the dope extrusion rate increases, the pore size re-

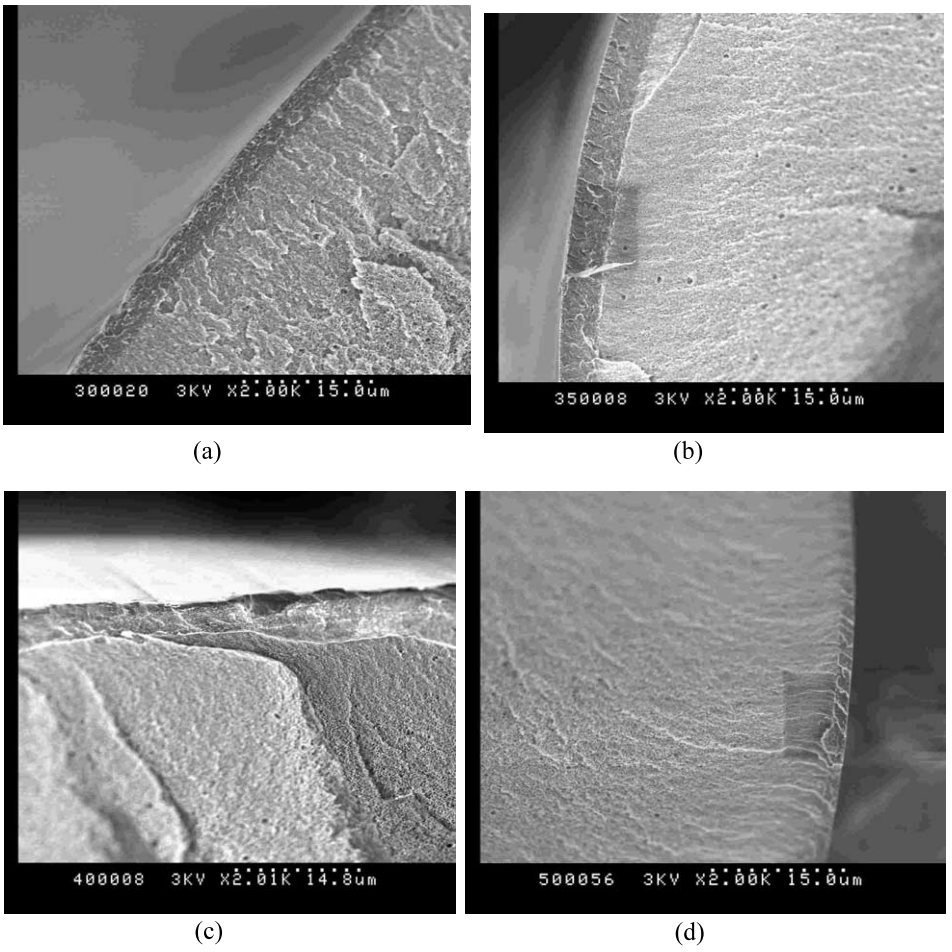


Fig. 2. Cross-sections of cellulose acetate hollow fibers spun at different shear rates: (a) 13479 $s^{-1}$ (b) 15726 $s^{-1}$(c) 17972 $s^{-1}$ (d) 22465 $s^{-1}$.

duces and the active skin layer decreases until a critical level of shear is reached. Beyond this shear rate, the pore size and the active layer no longer reduces but remains in this range. These modeling results are confirmed by the images taken from scanning electron microscope at magnification of 2000. The results seemed to be in line with the performance of the hollow fiber membranes, in another words they provided an explanation for the membrane performance. Hollow fibers spun at low shear rates tend to possess thicker skin and larger pore sizes, thus exhibiting the low rejections obtained. It seems that a thin active layer and small pore size correspond to high rejection rates. It is believed that the shear thinning behaviour of cellulose acetate dope solutions, which also exhibited viscoelasticity, resulted in polymer molecules becoming more aligned at greater shear [3,6,30]. This molecular orientation phenomenon has been studied and verified by means of the Fourier Transform attenuated total reflection (ATR) infrared dichroism [30] and also the polarized reflection infrared spectroscopy (DRIFTS) [3]. Since coagulation is most rapid at the membrane surface, these oriented polymer molecules may be 'frozen into', this surface region, forming the very thin skin

layer responsible for separation. However when extrusion shear rate gets beyond the critical shear value, pore size and the thickness of the membrane remains at this minimum value and this is reflected by the decrease in rejection rate. The results suggest that there seemed to be an optimum shear rate, which yields optimal membrane morphology. They are similar and consistent with those of Sharpe et al. [4] in the field of gas membranes and that of Qin and Chung [31] in ultrafiltration membranes.

The dip in rejection rates could probably be due to the development of surface defects. Although increasing the shear induces the molecular orientation, it also causes a reduction in skin thickness and strength, which eventually results in surface defects that undermine the enhancement in rejection rates. At the high level of shear, 17 972 $s^{-1}$, the apparent active layer thickness become very thin approximately 200 Å. This is so thin that slight imperfections may now begin to breach the skin.

The increase in the flux as shown in Fig. 3 suggests that the shear affects the phase inversion of the membrane active layer. The molecular orientation induced at the skin layer caused an increase in the free volume in the skin layer compared to the bulk polymer. According to Fritzsche et al. [32] the enhanced free volume in the skin layer contributes to increase flux rates across the membrane and this increase in free volume is reflected by an increase in glass transition temperature. The decrease in the calculated active layer thickness with increasing shear may be as a result of the way in which shear deformation interacts with the phase inversion process. The influence of rheology on phase inversion in membrane production and performance is an important aspect and has been studied by physical chemists such as Wolf [33], who has shown that shear can either increase or decrease phase stability, depending on the relative ability of the components in the system to store energy. In his early works [34], he discussed the distortion of the two-phase region in the phase diagram caused by shear.

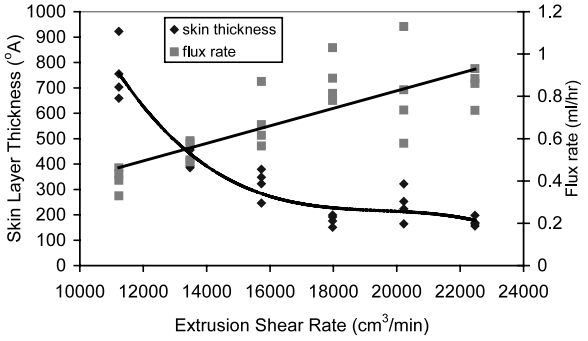


Fig. 3. Skin layer thickness and flux rate versus extrusion shear rate.

Cellulose acetate solution, which exhibits, shear thinning and viscoelastic behaviour, like other similar polymer systems has the ability to store energy increases with increasing viscosity, relaxation time and shear rate [34]. At high shear rates the polymer concentration increases in the system, resulting in diminishing increases in stored energy. Subsequently, this can result in an enlargement of the demixing region in the phase diagram, i.e. a decrease in stability, at increased rates [35]. Wolf and Kramer have used turbidimetric measurements to show that a shear field can increase the miscibility gap in macromolecular systems [35].

An enlargement of the miscibility gap that would almost certainly result in faster phase inversion. The decrease stability of the system apparently promotes a steeper polymer concentration gradient at the membrane surface; where the polymer poor phase would tend to be leaner and the polymer-rich phase would tend to be more concentrated. This situation where there exists more rapid coalescence of the polymer rich regions would set in place a thinner skin. Eventually, this would also provide the extra benefit of freezing in greater levels of molecular orientation more quickly to enhance rejection rates. This is consistent with the increase in flux and rejection rate with increasing shear rate in Table 2. However, after the critical shear rate of 17 972 $s^{-1}$ surface pores become detrimental to the rejection rates.

## 6. Conclusion

The modeling carried out allows fine structural details to be proposed that explain the performance of reverse osmosis hollow fiber membranes. This structural information also relates

hollow fiber performance to dope extrusion rates used during the spinning process. In conclusion:

(1) Dope extrusion shear rates determine the general morphology of a fiber: the pore size and the thickness of the active layer

(2) Rejection rates increases with increasing dope extrusion shear rates since the active skin thickness and pore size of membranes decreases. However, a critical shear rate exists beyond which membrane performance deteriorates probably due to the development of minor surface defects as the active layer thins.

(3) A minimum active layer thickness is desirable to maximize permeability.

(4) It is likely that shear affects the phase separation inversion dynamics of membrane precipitation as well as the orientation of the polymer molecules in the active layer.

## References

[1] S.J. Shilton, G. Bell, F. Ferguson, Deduction of fine structural details of gas separation hollow fiber membranes using resistance modeling of gas permeation, Polymer 37 (1996) 485–492.

[2] A.F. Ismail, Novel studies of molecular orientation in synthetic polymeric membranes for gas separation, PhD Thesis, University of Strathclyde, Glasgow, 1997.

[3] S.J. Shilton, A.F. Ismail, P.J. Gough, I.R. Dunkin, S.L. Gallivan, Molecular orientation and the performance of synthetic polymeric membranes for gas separation, Polymer 38 (9) (1997) 2200–2215.

[4] I.D. Sharpe, A.F. Ismail, S.J. Shilton, Study of extrusion shear and forced convection residence time in the spinning of polysulfone hollow fiber membranes for gas separation, Sep. Purif. Technol. 17 (2) (1999) 101–109.

[5] T.S. Chung, W.H. Lin, R.H. Vora, The effect of shear rates on gas separation performance of 6FDA-durene polyimide hollow fibers, J. Membr. Sci. 167 (2000) 55–66.

[6] S.A. Gordeyev, G.Y. Nikoleva, K.A. Prokhorov, R. Withnall, I.R. Dunkin, S.J. Shilton, P.P. Pashinin, Superselective polysulfone hollow fiber membranes for gas separation: assessment of molecular orientation by Raman spectroscopy, Modern Trends Laser Phys. 11 (1) (2001) 82–85.

[7] I. Ani, M.Y. Noordin, A.F. Ismail, S.J. Shilton, Study of shear rate influence on the performance of cellulose acetate reverse osmosis hollow fiber membranes, J. Membr. Sci. 5218 (2002) 1–11.

[8] I. Ani, A.F. Ismail, M.Y. Noordin, S.J. Shilton, Optimisation of cellulose acetate hollow fiber reverse osmosis membrane production using taguchi method, J. Membr. Sci., in press

[9] R. Wang, T.S. Chung, Determination of pore sizes and surface porosity and the effect of shear stress within a spinneret on asymmetric hollow fiber membranes, J. Membr. Sci. 188 (2001) 29–37.

[10] C.M. Tam, T. Matsuura, T.A. Tweddle, Polysulfone membrane: iii performance evaluation of PES–PVP membrane, Sep. Sci. Technol. 28 (1993) 2621–2633.

[11] S. Sourirajan, Reverse Osmosis, Logos Press Ltd, London, 1970.

[12] T. Matsuura, S. Sourirajan, Reverse osmosis transport through capillary pores under the influence of surface forces, Ind. Eng. Chem. Process. Des. Dev. 20 (1981) 273–282.

[13] T. Matsuura, Synthetic Membranes and Membrane Separation Processes, CRC Press, Boca Raton, FL, 1994, pp. 131–270.

[14] C. Bouchard, R. Lebrun, Synthesis of concentration polarisation and surface force–pore flow models in membrane separation, in: M. Malaiyandi, O. Kutowy, F. Talbot (Eds.), Proct. Int. Mem. Conf. 25th Anniv. Mem. Res., Canada, Ottawa, Canada, 24–26 September, 1986, pp. 295–311.

[15] D. Bhattacharyya, M. Jevtitch, J.T. Schrodt, G. Fairweather, Prediction of membrane separation characteristics by pore distribution measurements and surface force-pore flow model, Chem. Eng. Commun. 42 (1986) 111–128.

[16] B.J. Rudie, Nguyen, Calculation of the pore size distribution of PBI membranes, in: M. Malaiyandi, O. Kutowy, F. Talbot (Eds.), Proct. Int. Memb. Conf. 25th Anniv. Memb. Res., Canada, Ottawa, Canada, 24–26 September, 1986, pp. 295–311.

[17] L. Tinghul, K. Chan, T. Matsuura, S. Sourirajan, Determination of interaction forces and average pore size and pore size distribution and their effects on fouling of ultrafiltration membranes, Ind. Eng. Chem. Prod. Res. Dev. 23 (1984) 116–124.

[18] S.K. Gupta, Design and analysis of reverse osmosis systems using 3 parameter models for transport across the membranes, Desalination 85 (1992) 283–290.

[19] C.S. Zhao, X. Xhou, Y. Yue, Determination of pore size and pore size distribution on the surface of hollow fiber filtration membranes; a review of methods, Desalination 129 (2000) 107–123.

[20] W. Pusch, Performance of reverse osmosis membranes in correlation with membrane structure, transport mechanisms and module design (fouling); state of the art, Desalination 77 (1990) 35–54.

[21] J.M. Dickson, J. Spencer, L.M. Costa, Dilute single and mixed solute systems in a spiral wound reverse osmosis module part 1 theoritical model, Desalination 89 (1992) 63–70.

[22] B.A.Q. Darwish, G.S. Aly, Al. Rqoobah, A. Jawad, Desalination 75 (1989) 55–62.

[23] M. Brusilovsky, D. Hassan, Desalination 71 (1989) 355.

[24] S. Velikova, A.M. Dave, V. Mavrov, M.H. Mehta, Comparative evaluation of industrial membranes: correlation between transport and operational parameters, Desalination 94 (1993) 1–10.

[25] N.G. Voros, Z.B. Maroulis, D. Marinos-Kouris, Salt and water permeability in RO membranes, Desalination 104 (1995) 141–154.
[26] Y. Wang, W.L. Wayne, S. Sourirajan, Effects of pretreatments on morphology and performance of cellulose acetate (formamide type) membranes, Desalination 95 (1994) 155–169.
[27] I. Ani, A.F. Ismail, S. Iswandi, S.J. Shilton, Effect of methanol on the performance of asymmetric cellulose acetate reverse osmosis membranes using dry/wet phase inversion technique, J. Teknol. 34 (2001) 39–50.
[28] S.J. Shilton, G. Bell, J. Ferguson, The rheology of fiber spinning and the properties of hollow fiber membranes for gas separation, Polymer 35 (1994) 5327–5334.
[29] D. Bhattacharyya, M.E. Williams, Reverse osmosis (theory), in: W.S. Winston, K. Sirkar (Eds.), Membrane Handbook, Van Nostrand Reinhold, New York, 1992, pp. 266–280.
[30] I. Ani, M. Noorhayati, A.F. Ismail, S.J. Shilton, Measurement of rheologically induced molecular orientation using ATR in RO hollow fiber cellulose acetate membranes and influence on separation performance, J. Membr. Sci., submitted for publication.
[31] J. Qin, T.S. Chung, Effect of dope flow rate on the morphology, separation performance, thermal and mechanical properties of ultrafiltration hollow fiber membranes, J. Membr. Sci. 157 (1999) 35–51.
[32] A.K. Fritzsche, M.K. Murphy, C.A. Cruse, R.F. Malone, R.E. Kesting, Characterisation of asymmetric hollow fiber membranes with graded-density skin, Gas Sep. Purif. 3 (1989) 106.
[33] B.A. Wolf, Thermodynamic theory of flowing polymer solutions and its application to phase separation, Macromolecules 17 (1984) 615.
[34] B.A. Wolf, Improvement of polymer solubility influence of shear and pressure, Pure Appl. Chem. 9 (1997) 929–935.
[35] B.A. Wolf, H. Kramer, Phase separation of flowing polymer solutions studied by viscosity and by turbidity, J. Polym. Sci. Lett. 18 (1980) 789.